Controlling the Selectivity of Supported Ru Nanoparticles During Glycerol Hydrogenolysis: C–O *vs* C–C Cleavage

Susana Guadix-Montero,[a] Alba Santos Hernandez,[a] Nian Lei,[b] David J. Morgan,[a] Qian He,[a, c] Aiqin Wang,[b, d] Tao Zhang,[b] Alberto Roldan,*[a] and Meenakshisundaram Sankar*[a]

Controlling the selectivity of a reaction by rational designing of catalyst is an important and challenging topic in catalysis research. In this article, we report a strategy to tune the product selectivity during aqueous phase hydrogenolysis of glycerol using gaseous H_2. Ru/TiO_2 is an active catalyst for the hydrogenolysis of glycerol, however it promotes the hydrogenolysis of C–C bonds resulting in large quantities of C2 and C1 products. On the other hand, Pd/TiO_2 and Pt/TiO_2 catalysts are very selective for the hydrogenolysis of C–O bonds producing mainly C3 products (1,2 and 1,3 propanediols), however they are much less active compared to the Ru catalysts. In this article, we report that by combining Ru with Pt or Pd in a bimetallic nanoparticle, we can develop new catalysts that are both active and selective for C–O hydrogenolysis. A physical mixture of two monometallic catalysts does not show this enhanced selectivity for C–O hydrogenolysis, proving that intimate mixing of the two metals in a nanoparticle is crucial to tune the selectivity. All the monometallic and bimetallic catalysts have been characterised by microscopic and spectroscopic methods to understand their structural features. DFT studies were also done to rationalise the observed difference in the catalytic properties between monometallic and bimetallic catalysts.

Introduction

Hydrogenolysis of bioderived platform molecules has received considerable attention in an effort to find a green and sustainable alternative to fossil fuel-based feedstock to produce fine chemicals and fuels.[1] Glycerol, a by-product from biodiesel production, is one of the platform molecules identified by the US Department of Energy (DoE) that has the potential to replace current feedstock to produce bulk chemicals.[2] Valorisation routes such as selective oxidation, selective hydrogenolysis, dehydration and many more have been reported for the conversion of glycerol to more value-added products.[1e,3] Among these routes, hydrogenolysis of glycerol (Scheme 1) to propanediols (PDOs) such as 1,2-propanediol (1,2-PDO) and 1,3-propanediol (1,3-PDO) has received considerable attention because of the commercial importance of PDOs.[1d,4] They are used in the production of unsaturated polyester resins, food additives, paints, cosmetics, liquid detergents, print ink, plasticizers, anti-freeze, de-icing and heat transfer fluids.[1c] Currently, PDOs are produced either by the chlorohydrin process or hydroperoxide process involving propylene oxide derived from fossil fuel-based feedstock.[1d,e] Hence, the development of an active and stable catalyst for the selective hydrogenolysis of glycerol to form PDOs is crucial to realise our ambition to produce fuels and chemicals from renewable feedstock. During the hydrogenolysis of glycerol, the selectivity for PDOs depends on the selective hydrogenolysis of C–O bond over C–C bond which results in C2 (ethylene glycol, ethanol) and/or C1 (methanol and methane) products. A number of transition metal (Ru, Rh, Re, Pt, Pd, Ir, Ag, Cu, Co and Ni) catalysts have been reported for the hydrogenolysis of glycerol.[1b–e,4a,5] For different metals the selectivity for C–O bond hydrogenolysis follows the order Ru < Rh < Pt < Pd, however the reverse order has been reported for the C–C hydrogenolysis.[6] Hence, it is challenging to design a catalyst for selective PDO production without compromising the catalytic activity.

Since the development of bimetallic catalysts for reforming reactions by Sinfelt,[7] several research groups have developed a number of bimetallic catalysts for a variety of chemical transformations.[8] Addition of second metal to a primary metal, to form bimetallic nanoparticles, can alter its catalytic properties.[8–9] Hutchings and co-workers have reported the superiority of bimetallic AuPd catalysts for several reactions including direct synthesis of hydrogen peroxide, solvent free oxidation of primary alcohols and selective oxidation of

[a] S. Guadix-Montero, A. Santos Hernandez, D. J. Morgan, Q. He, Dr. A. Roldan, Dr. M. Sankar
Cardiff Catalysis Institute, School of Chemistry
Cardiff University
Cardiff CF10 3AT (United Kingdom)
E-mail: RoldanMartinezA@cardiff.ac.uk
sankar@cardiff.ac.uk
[b] N. Lei, A. Wang, T. Zhang
State Key Laboratory of Catalysis
Dalian Institute of Chemical Physics
Chinese Academy of Sciences
457 Zhongshan Road, Dalian, Liaoning 116023 (P. R. China)
[c] Q. He
Department of Materials Science and Engineering
National University of Singapore
Singapore, 117575 (Singapore)
[d] A. Wang
Dalian National Laboratory for Clean Energy
457 Zhongshan Road, Dalian 116023 (P. R. China)

Supporting information for this article is available on the WWW under https://doi.org/10.1002/cctc.202001881

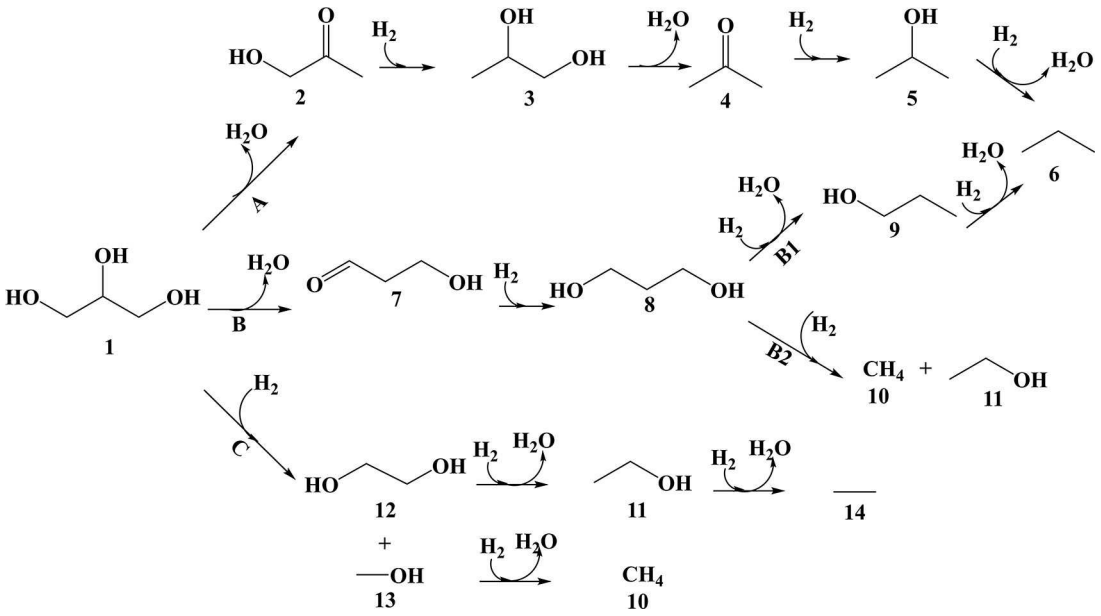

Scheme 1. Schematic representation of the glycerol hydrogenolysis reaction pathways. Compounds labelled as. 1) glycerol, 2) acetol, 3) 1,2-propanediol, 4) acetone, 5) 2-propanol, 6) propane, 7) 3-hydroxypropanaldehyde, 8)1,3-propanediol, 9)1-propanol, 10) methane, 11) ethanol, 12) ethylene glycol, 13) methanol, 14) ethane. Adapted from reference.[16]

glycerol.[10] Falcone *et al.* reported the beneficial effect of the bifunctional bimetallic Pt–Re catalyst to increase the selectivity of 1,3-PDO during the hydrogenolysis of glycerol.[11] Initially, they improved the activity of monometallic 8 wt.% Pt/SiO_2 ($TOF = 4.2 \times 10^{-6}\,s^{-1}$) by the addition of HCl ($TOF = 5.5 \times 10^{-5}\,s^{-1}$) and then by incorporating Re (0.0105 s^{-1}). Luo *et al.* reported that, for the hydrogenolysis of levulinic acid (LA) to *gamma*-valerolactone (GVL), bimetallic AuPd catalyst (TOF 0.1 s^{-1}) is several folds more active that the corresponding monometallic Au and Pd catalysts (Au, TOF 0.004 s^{-1} and Pd, TOF 0.005 s^{-1}).[12] In the same article, they further reported that the most active and unselective Ru/TiO_2 catalyst could be transformed to a highly selective catalyst by the addition of Pd and blocking the unselective sites.[12] Salazar *et al.* reported that the incorporation of Cu to monometallic Ru/TiO_2 catalyst increased the selectivity of 1,2-PDO from 48 to 69% at the expense of EG selectivity (41 to 25%), and glycerol conversion (19 to 10%).[13] The synergistic effect of Ru and Re on TiO_2 was reported by Ma *et al.* who reported that the bimetallic RuRe showed higher selectivity for C3 products, in addition to higher activity, compared to the monometallic Ru catalysts due to better dispersion of the bimetallic RuRe nanoparticles.[14] Maris *et al.* reported an increase in the stability of bimetallic RuPt/C catalyst compared to the monometallic Ru/C catalyst.[15] However, these catalysts, including monometallic Ru catalysts are active at higher temperatures or pressures. For glycerol hydrogenolysis the challenge is to find an efficient catalyst that is active at milder reaction condition, that selectively breaks C–O bonds without breaking the C–C bonds. Here, we report that by adding Pt or Pd to an active Ru/TiO_2 catalyst a dramatic increase in the selectivity of C3 can be achieved. We attempt to rationalise this interesting synergistic effect for the bimetallic catalysts using advanced spectroscopic and microscopic characterisation and by density functional theoretical studies.

Experimental Section

Catalyst preparation

Monometallic Pd, Ru, Pt and bimetallic RuPd, RuPt nanoparticles supported on TiO_2 were prepared *via* a modified impregnation method.[12,17] In a typical catalyst preparation, 2 g of 2 wt.% RuPd/TiO_2 catalyst with equal molar loadings of the two metals was prepared. Prior to the catalyst preparation, metal stock solutions were analysed using an Agilent 4200 MP-AES instrument to quantify the metal concentration. A precursor solution of $PdCl_2$ (99%, Aldrich) was prepared with a metal concentration of 6 $mg_{Pd}\,mL^{-1}$ in a 0.58 M HCl aqueous solution. An aqueous solution of $RuCl_3.xH_2O$ (> 99.9%, Aldrich) with a metal concentration of 6.7 $mg_{Ru}\,mL^{-1}$ was also prepared separately. Requisite amounts of metal precursor solutions were added to a 50 mL round-bottom flask fitted with a magnetic stirrer bar. Additional volume of deionised water was added to make the total volume of the impregnation mixture to 16 mL and the solution was stirred vigorously, while the temperature of the solution was increased from room temperature to 60 °C. At 60 °C, the support (Degussa P-25 TiO_2 −1.98 g) was added slowly over a period of 15–20 min with constant stirring. The slurry was stirred at 60 °C for an additional 15 min, followed by an increase in temperature to 95 °C. The slurry was stirred overnight until all the water evaporates (typically 16 h). Subsequently, the resultant dry powder was ground thoroughly and reduced at 400 °C (heating rate = 10 °C min^{-1}) for 4 hours under a constant flow of 5% vol. H_2/Ar.

Glycerol hydrogenolysis

Batch reactor

The hydrogenolysis of glycerol over supported monometallic and bimetallic nanoparticles were performed in a 50 mL stainless-steel autoclave (Parr® Instruments) reactor with a maximum operating pressure of 2000 psi using molecular H_2. This autoclave reactor is equipped with an overhead magnetic stirrer (0–1500 rpm). The reaction temperature was monitored using a thermocouple and the reactor pressure was measured using a transducer fitted in the autoclave reactor. The reactor was charged with an aqueous solution of glycerol (24 mL of 5 wt.% glycerol solution), catalyst with a constant total metal: substrate molar ratio (1:200). In a typical reaction, the autoclave was initially purged 3 times with N_2 (10 bar) followed by further purging (2 times) with H_2 (20 bar) and then finally pressurized at 20 bar at 25 °C. Then the heating of the reactor was started. Initially, the reaction mixture was stirred at < 200 rpm until the reaction temperature reached 165 °C, after that, the reaction mixture was stirred vigorously at *ca.* 800 rpm and this point was noted as the starting point of the reaction. At the end of the reaction, the reactor was cooled in an ice bath until the temperature of the reaction mixture reaches 25 °C. The gas phase products were collected in a gas sampling bag (temperature and pressure were measured for quantitative analyses) and were injected in a Varian 450-GC, fitted with a Varian Capillary Column (CP-Sil 5 CB 50 m 0.32 mm 5 μm). After the gases are separated in the column, it passes through a methaniser - which contains a nickel catalyst at a high temperature and H_2 which converts CO_2 to methane and then by a flame ionization detector (FID). The gaseous products (carbon dioxide and methane for C1 products, ethylene for C2 products and propane for C3 products) were quantitatively analysed using appropriate response factors were obtained by injecting different volume % of the standard gas mixtures of known concentrations, which allows getting the molar fraction of each gas in the sampling bag. The moles of each component in the gaseous phase were then calculated using the Dalton's law of partial pressures and the ideal gas equation. The volume of gas in the reactor was estimated by the total volume of the reactor subtracted by the volume of the liquid reaction mixture.

For liquid-phase analysis, the solid catalyst was removed from the liquid reaction mixture using a centrifuge at 4300 rpm for 20 min following by filtration using a 0.45 μm PTFE syringe filter. An aliquot of the liquid reaction mixture along with a fixed amount of external standard (*n*-butanol) was injected in a GC (Agilent 7820 A) fitted with an Agilent DB-WAX Ultra Inert GC column and a flame ionization detector. Quantitative analyses of the substrates and products were performed with the help of calibration plots and response factors for all the liquid products identified to work out the moles of each component. The conversion, selectivity and total carbon mass balance (CMB(T)) was calculated using the following equations, note that the moles of each compound were multiplied by the number of carbons present in that component to determine the C content. The final conversion and C selectivities were calculated from the data obtained from the two independent liquid phase and gas phase analyses.

$$Conversion\ (\%) = \frac{(mol_{glycerol})_{t=0} - (mol_{glycerol})_{t=t}}{(mol_{glycerol})_{t=0}} \cdot 100 \quad (1)$$

$$Selectivity_P\ (\%) = \frac{number\ of\ carbons\ atoms\ of\ P\ \cdot\ mol_P}{\sum mol_{C1\ products} + 2 \cdot \sum mol_{C2\ products} + 3 \cdot \sum mol_{C3\ products}} \cdot 100 \quad (2)$$

$$Total\ carbon\ mass\ balance\ (\%) = \frac{\sum mol_{C1\ products} + 2 \cdot \sum mol_{C2\ products} + 3 \cdot \sum mol_{C3\ products} + 3 \cdot (mol_{glycerol})_{t=t}}{3 \cdot (mol_{glycerol})_{t=0}} \cdot 100 \quad (3)$$

For reusability studies, at the end of the reaction, the catalysts were filtered, washed with acetone several times, and dried at 25 °C overnight. These dried catalysts were dried further in an oven at 120 °C in static air for 1 h and used for the next reaction. The dried only catalysts were used for characterisation.

Fixed-bed reactor

Glycerol hydrogenolysis was also done in a fixed-bed column reactor (9 mm-ID x 400 mm-High) provided with a heating jacket, a MFC (mass flow controller) and connected to a gas-liquid separator (Figure 1). In a typical reaction, 0.5 g of the catalyst pellets (20-40 mesh) were loaded mixed with 0.5 g of SiO_2 (20–40 mesh, purchased from Tianjin Tianda Chemical Reagent Co. Ltd) and fitted with glass wool at the centre of the column. The column was packed with a total of *ca.* 52 g of SiO_2 and the reactor was purged with N_2 at the max flow (500 mL min^{-1}). The reactor temperature was increased at a rate of 5 °C min^{-1} until it reached the set reaction temperature. After stabilising the reactor temperature at 165 °C, 20 wt.%, aqueous glycerol solution was fed into the reactor (1 mL min^{-1}). The space velocity was worked out using the Weight hourly space velocity (WHSV) = Hourly mass feed flow rate/ Catalyst mass. Therefore, different flow rates were used depending on the catalyst tested in order to use constant weight of all the catalysts tested (0.5 g) with a constant metal-to-substrate molar ratio at 1:200. The gas phase products were analysed directly by an on-line GC (Packed column) directly, while an aliquot of the liquid products was sampled manually from the liquid-gas separator and analysed in an offline GC (Agilent 7820 A) fitted with an Agilent DB-WAX GC column and a flame ionization detector, after diluting it with the external standard (*n*-butanol).

Catalyst characterisation

Thermogravimetric Analyses: Thermogravimetric analyses (TGA) studies of the fresh and spent Ru/TiO_2, $RuPt/TiO_2$ and $RuPd/TiO_2$, were performed in a PerkinElmer Pyris 1 thermogravimetric analyser, under a N_2 flow of 30 mL min^{-1}, the samples were stabilised at 30 °C for 20 min. After stabilisation, the temperature was increased to 800 °C at a rate of 10 °C min^{-1}. No corrections for gas buoyancy effects were applied. In this article, only the relative intensities are reported.

X-ray Photoelectron Spectroscopic (XPS) studies

Elemental analysis and atomic oxidation states of the just reduced Ru/TiO_2, $RuPt/TiO_2$ and $RuPd/TiO_2$ catalyst surfaces were performed on a Thermo Scientific™ K-Alpha$^+$ X-ray photoelectron spectrometer (XPS) utilising monochromatic Al radiation operating at 72 W power at a spot size of 400 microns. Dual low energy electron and Ar^+ neutralisation was used, and all data calibrated to the C(1 s)

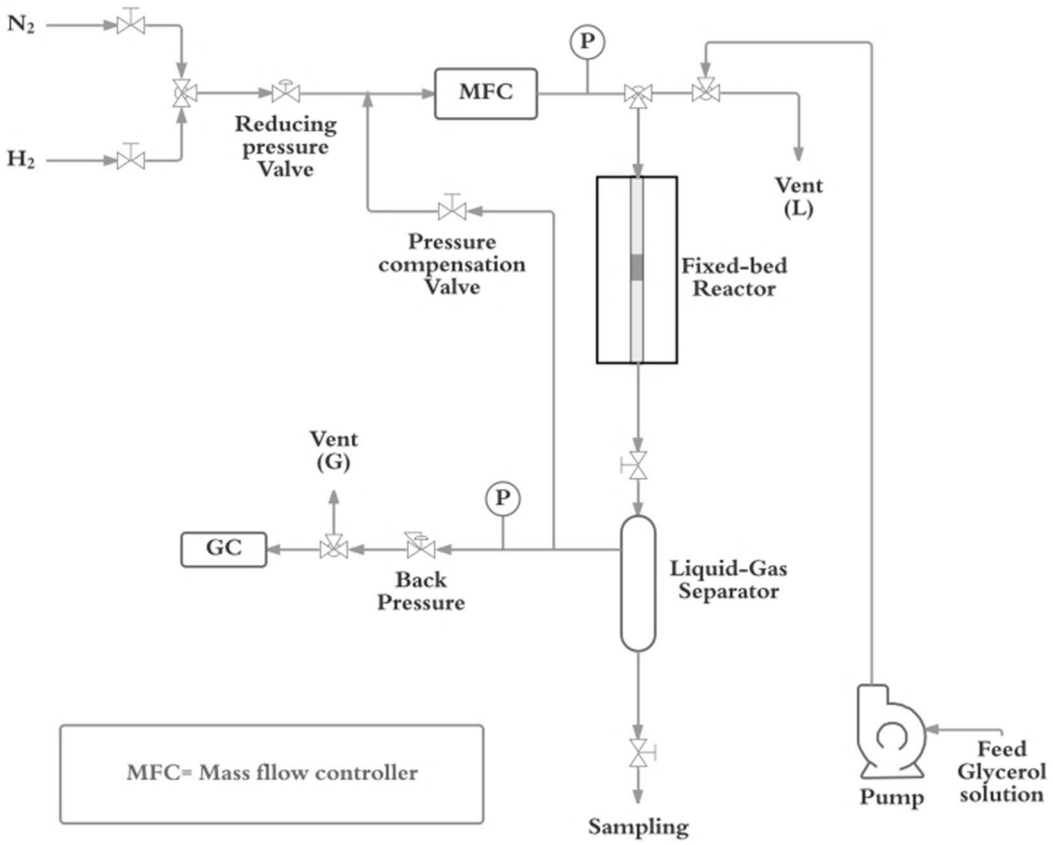

Figure 1. Schematic representation of the fixed bed reactor used for glycerol hydrogenolysis.

line at 284.8 eV when required. All the XPS data were analysed using CasaXPS using Scofield sensitivity factors corrected with an energy dependence of 0.6 eV, after application of a Shirley background (see supporting information).

Scanning Transmission Electron Microscopic (STEM) studies

The metal particle size distribution of the 2% Ru/TiO_2 , $Ru–Pt/TiO_2$ and $RuPd/TiO_2$ catalysts were obtained on a Transmission Electron Microscope (JEM-2100F (JEOL)). Prior to the TEM analysis, samples were dispersed with ethanol under ultrasonication. Supernatant liquid was dropped on a C-grid and dried using a lamp before analysis. STEM-EDX mapping was carried out and analysed by Oxford Instrument.

Inductively coupled plasma mass spectroscopy

The liquid samples were analysed using an Agilent Technologies 7900 ICP-MS system, fitted with an Agilent Integrated Autosampler. Quantitative data were obtained using internal standards and standard calibration plots.

Computational details

Slab calculations were performed using the Vienna ab initio simulation package (VASP),[18] with the exchange - correlation described by the PBE density functional,[19] and a plan wave kinetic energy cut-off of 450 eV. The inner electrons were represented by projector augmented wave (PAW) pseudopotentials.[20] The calculated lattice parameters for Ru, Pd and Pt are 2.688, 3.880, and 3.915 Å, respectively, and $[c/a]_{Ru} = 1.585$, in good agreement with experimental values of 2.706, 3.893, and 3.924 Å and $[c/a]_{Ru} = 1.582$.[21] Different fcc 50:50 homogeneous alloys arrangements were considered and their lattice optimised, and only the most stable configuration was used to study the molecular adsorptions, see Figure 2. A five-layer slab were built by p(4×4) and the molecule absorbed on different arrangements. The two topmost layers were fully relaxed, and the three bottom layers were fixed to the optimised bulk distances. For surface calculations, the Brillouin zone was sampled by a 5x5x1 Γ-centered *k*-point mesh generated through the Monkhorst–Pack method.[22] We included a vacuum region larger than 14 Å and a dipole correction along the *z*-direction upon molecular absorptions.[23] We also included the van der Waals (vdW) corrections by applying Grimme's DFT–D3 method.[24] The molecules in the gas phase were relaxed in a broken-symmetry box of 15×16×17 $Å^3$. The optimization thresholds were 10^{-5} eV and 0.03 eV/Å respectively for electronic and ionic relaxations.

The relative energies between the different surface species were calculated relative to the pristine surface and the isolated gas phase glycerol, see eq. 4

$$\Delta E = E_{surface\ species} - (E_{pristine\ surface} + E_{glycerol}) \quad (4)$$

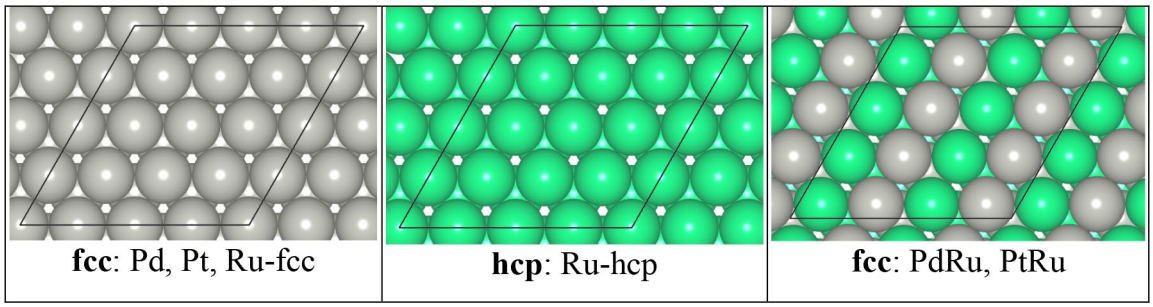

Figure 2. Representation of fcc and hcp structures of the catalysts' most stable surface. Black frame indicates the simulation periodic cell.

Results and Discussion

2 wt.% of monometallic Pd, Ru, Pt and bimetallic RuPd, RuPt (equimolar metal ratio) nanoparticles supported on TiO_2 were tested for the hydrogenolysis of glycerol at 165 °C for 16 h in a batch reactor. Two different monometallic catalysts, with the same mols of metal as that of bimetallic catalysts, were physically mixed and tested under identical reaction conditions for comparison. The catalytic results (Figure 3) clearly show that, for the monometallic catalysts, the catalytic activity follows the trend Ru > Pt > Pd, which is in agreement with previous reports,[6] achieving glycerol conversion of 89, 20 and 5%, respectively. However, the selectivity for C3 products follows the opposite order, with >95% selectivity for both Pd and Pt and only a 30% for Ru. Figure 3 further shows a marginal increase in the selectivity for C3 products when monometallic Pd or Pt catalysts were physically mixed with the monometallic Ru catalyst (from 30% to *c.a.* 35–40% in both cases). However, when bimetallic RuPd and RuPt catalysts were used, a substantial increase in C3 products selectivity was observed (58% and 65% for RuPd and RuPt respectively). Detailed products selectivity data and carbon balance for all these catalytic reactions are presented in the supporting information (Table S1 and Table S2).

The yield of degradation products (C1 + C2) was >60% for the monometallic Ru catalyst and >50% for the physically mixed catalyst system. However, for the bimetallic catalysts (RuPd and RuPt) this value was much lesser (between 20–24%). Detailed product selectivity and yields for all the catalysts are given in the supporting information (Table S1). These data clearly show that the bimetallic catalysts show better selectivity for C–O bond hydrogenolysis (C3 compounds) without compromising the catalytic activity excessively. For the bimetallic catalysts, 1,2-PDO is the major C3 product with an overall product selectivity of *ca.* 46–50% (Table S2 in supporting information). The catalytic behaviour of the two physically mixed Ru + Pd and Ru + Pt catalysts resembled the monometallic Ru catalyst than the bimetallic catalysts, indicating that the

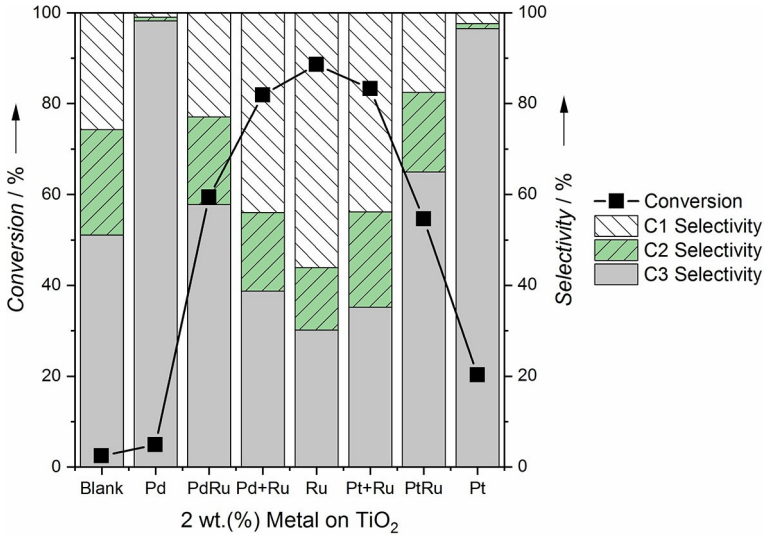

Figure 3. Comparison of catalytic activities of supported monometallic and bimetallic (2 wt. % Pd, Pt, Ru, RuPd, and RuPt on TiO_2) nanoparticles for the hydrogenolysis of glycerol in an autoclave batch reactor. Where RuPd and RuPt correspond to the bimetallic nanoparticles and the Ru + Pd and Ru + Pt correspond to physically mixed two monometallic catalysts. Selectivity of products classified as: C1 (methanol, methane and carbon dioxide), C2 (ethanol, ethylene glycol and ethane), C3 (acetol, 1,2-propanediol, acetone, 2-propanol, propane, 1,3-propanediol and 1-propanol). Reaction conditions: temp: 165 °C; time: 16 h; pH_2: 20 bar, stirring speed: 800 rpm; metal to glycerol molar ratio 1:200, in a batch reactor.

intimate mixing of the two metals at a nanoscale is crucial to enhance the selectivity. The proposed pathway for monometallic Ru catalyst is either pathway **C** or **B** (Scheme 1), leading to C–C bond cleavage, evidenced by high glycerol conversion (89%) to gaseous products, such as methane, ethane, propane.[25] Monometallic Ru catalyst showed a Carbon Mass Balance for the liquid products (CMB(L)) of 36%, remaining gaseous products. On the other hand, monometallic Pd and Pt catalysts displayed low conversions (*ca.* 5% and 20%, respectively) with higher percentage of liquid products (*ca.* 86–97% of CMB(L), see supporting information Table S2). Interestingly, both bimetallic catalysts gave relatively high glycerol conversion (above 50%), with very high CMB(L) (*c.a.* 90% for RuPt and 82% for RuPd). Compared to monometallic Ru catalyst, bimetallic catalysts suppress nearly 50% of the C1 & C2 products.

Time on line catalytic studies for the monometallic Ru and bimetallic RuPd and RuPt catalysts were performed in a batch reactor (Figure 4). The results are presented and discussed using three CMB values: carbon mass balance for liquid products (CMB(L)), carbon mass balance for gaseous products (CMB(G)) and total carbon mass balance (CMB(L + G)). Detailed products distribution data for all these reactions is presented in the supporting information (Table S3).

Among all the catalysts tested, monometallic Ru/TiO_2 catalyst is the most active catalyst showing excellent glycerol conversion (*ca.* 47% in 1 h and *ca.* 81% in 6 hours (Figure 4A,)), however, predominantly to C1 and C2 products (selectivity after 6 h CH_4: 51%; 1,2-PDO: 21%; EG: 11% and C_2H_6:7%). Among the liquid products, 1,2-PDO has higher selectivity (*ca.* 21–26% % at 1 and 16 h of reaction) followed by EG with a selectivity of 11% at 6 h but decreasing to 6% after 16 h. From 1 to 16 h, the CMB (L) decreased from *ca.* 70% to 35% because of the formation of gaseous products as shown Table S3. This data suggests that monometallic Ru catalyst promotes C–C bond cleavage *via* the pathway **C**, where CH_4 is a major product, (*i.e.*, *ca.* 85% of the gaseous products), and more than 50% of overall carbon selectivity after 6 h (Table S3). Compared to other monometallic Ru catalysts reported in the literature, this is one of the most active monometallic Ru catalysts (a comparison is presented in supporting information Table S4 & S5). The superior activity of this Ru catalyst, prepared by the modified impregnation method, is because of smaller Ru nanoparticles combined with good dispersion (discussed later). All the reported monometallic Ru catalysts are effective for C–C hydrogenolysis (supporting information, Table S5).

The bimetallic $RuPt/TiO_2$ showed a lower rate of glycerol conversion (Figure 4B), however, the selectivity for liquid products was much higher (CMB(L) around 90%) compared to the monometallic Ru catalyst (CMB(L) = 36%). For both monometallic Ru and bimetallic RuPt catalysts, 1,2-PDO is the most selective liquid product. However, $RuPt/TiO_2$ gave a higher 1,3-PDO selectivity (*ca.* 10–13%) compared to Ru/TiO_2 catalyst (0–2%), suggesting the promotion of the hydrogenolysis reaction pathway **B** (Scheme 1) by the bimetallic catalyst. This is further supported by the production of 1-propanol (*ca.* 10% throughout the reaction) formed *via* further dehydration of 1,3-

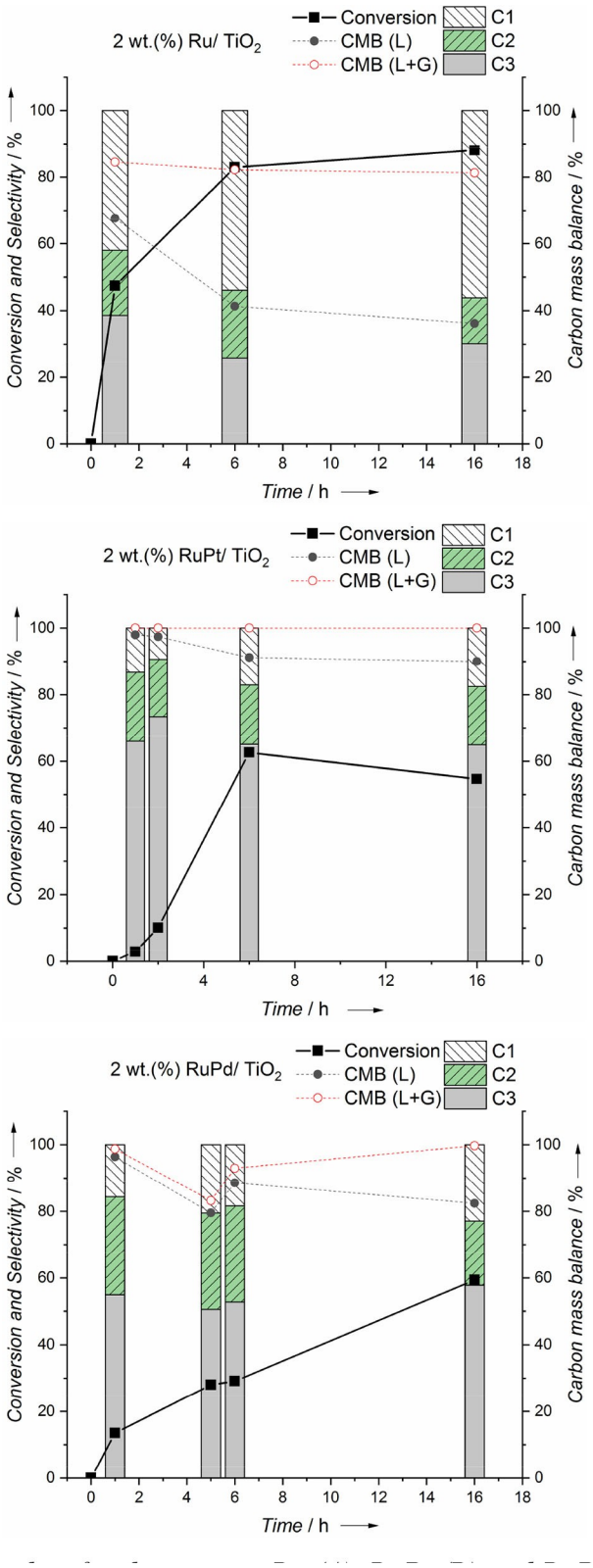

Figure 4. Kinetic studies for the 2 wt. % Ru (A), RuPt (B) and RuPd (C) supported on TiO_2 at 165 °C; pH_2: 20 bar, 800 rpm; metal to glycerol molar ratio of [1:200] in a batch reactor. Conversion, total carbon mass balance (L + G) and selectivity of products label as: C1 (methanol, methane and carbon dioxide), C2 (ethanol, ethylene glycol and ethane), C3 (acetol, 1,2-propanediol, acetone, 2-propanol, propane, 1,3-propanediol and 1-propanol).

propanediol. The selectivity of EG decreased with time from 15% to 7.5%, whilst ethanol, formed *via* a C–C cleavage of 1,3-propanediol (pathway **B2)**, showed a constant *ca.* 5% selectivity. Though bimetallic RuPt/TiO_2 produces higher percentage of C3 compounds than the monometallic Ru/TiO_2 catalyst, it still produces C2 and C1 products and their concentration increases with reaction time (supporting information Table S3). The second bimetallic RuPd/TiO_2 catalyst gave *ca.* 60% conversion after 16 h (Figure 4C), however, the CMB(L) was much higher (80–85%) than the monometallic Ru/TiO_2 catalyst (36%) but less than that of RuPt/TiO_2 catalyst (90%)(supporting information Table S3). Among the liquid products, 1,2-PDO is the most selective product with its selectivity increasing from 44% in 6 h to 50% after 16 h resulting in a *ca.* 30% yield. This suggests that RuPd catalyst promotes the thermodynamically favourable dehydration reaction pathway **A** (Scheme 1) involving the acetol intermediate which hydrogenates to form 1,2-PDO, however only small amounts of this acetol intermediate was detected.[26] With increasing reaction time from 1 to 16 h reaction, the EG selectivity reduced from *ca.* 25% to 13%. The selectivity of 1-PO also decreased from 7% in 1 h to 4% in 16 h, due to further hydrogenolysis of it to form gas products. Both bimetallic catalysts produce significantly higher proporption of C3 compounds (almost twice) compared to their analogous monometallic catalysts. Table S6 & S7 (supporting information) shows that these bimetallic catalysts are some of the most active catalysts reported so far. It must be noted that some of the reaction conditions and analyses methodologies are different in the reported literature. Hence the comparison should be made carefully.

Comparison of products selectivity between different monometallic and bimetallic catalysts at iso conversion levels (Figure S1 in supporting information) suggests that the C–C vs C–O selectivity is not a function of conversion. The conversion for monometallic Pd was *ca.* 5% after 16 h, however the conversation for monometallic Ru catalyst, at similar reaction conditions, was substantially higher, hence 50% less catalyst loading was employed to achieve comparable conversion. For the comparison of activities between monometallic Pt and Ru catalysts, a similar strategy was employed. Data from Figure S1 show that monometallic Ru catalyst produced higher C–C hydrogenolysis products (< C3), compared to monometallic Pd and Pt catalysts who showed 78 and 69% selectivity towards 1,2-PDO, respectively (Supporting information Figure S1) at iso-conversion levels. This clearly indicates that monometallic Ru catalyst promotes C–C bond hydrogenolysis whereas monometallic Pd and Pt catalysts promote C–O bond hydrogenolysis. This is in line with earlier reports.[6] The selectivity for monometallic Ru catalyst was also compared with the bimetallic RuPd and RuPt catalysts at isoconversion levels (Figure S1). Bimetallic catalysts achieved much higher selectivity for 1,2-PDO (50%) in comparison to monometallic Ru catalyst (25%) at *ca.* 50% conversion.

Figure 5 shows the preliminary reusability data for the bimetallic catalysts in a batch reactor. RuPt/TiO_2 catalyst deactivates with every use, whereas RuPd/TiO_2 appears to be stable for at least 2 re uses in a batch reactor. The reusability of these catalysts was also investigated in a continuous flow fixed bed reactor. The catalytic results (Figure S2, supporting information) followed a similar trend to what we observed in the batch reactor - such as monometallic Ru catalyst more active producing substantial amount of gaseous products, whereas bimetallic catalysts are selective towards C3 products. For a reasonable comparison of the catalytic data between the batch and the continuous reactors, the Space Time (ST)[27] was calculated for the batch and continuous reactions using the equations (5) and (6) respectively:

$$ST = \frac{mass\ of\ catalyst\ (g_{cat})}{mass\ of\ glycerol\ (g_{glycerol})} \times reaction\ time\ (h) \tag{5}$$

$$ST = \frac{mass\ of\ catalyst\ (g_{cat})}{glycerol\ mass\ flow\ rate\ (g_{glycerol}/h)} \tag{6}$$

The activities of all the monometallic and bimetallic catalysts in the fixed-bed reaction were compared with the activities in the batch reactors at equivalent STs (see the ST

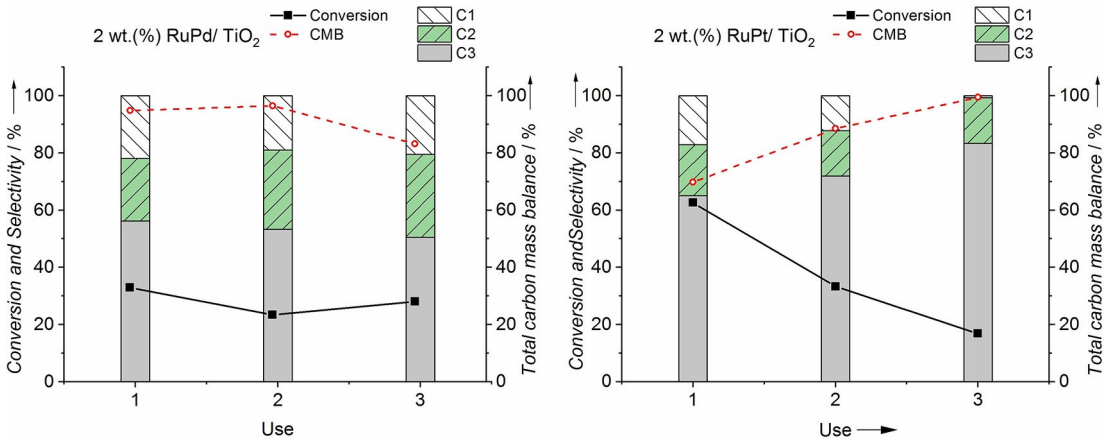

Figure 5. Reusability study for the bimetallic catalysts on TiO_2 in a batch reactor. PdRu alloy 5 hour of reaction each use (left hand side), while RuPt was run for 6 h of reaction each use (right hand side).

Table 1. Catalyst and reactant charges for both reactor configurations. ST for 6 h of reaction time.

2wt.% Metal/TiO_2	*ST*, $\frac{g_{catalyst} \cdot h}{g_{reactant}}$	*Batch* mass catalyst [g]	mass glycerol [g]	*Fix-Bed* mass catalyst [g]	glycerol [g/h]	Glycerol solution [g/h]	Pump Flow [mL/min]
Ru	1.645	0.329	1.2	0.5	0.304	1.514	0.0200
RuPt	2.415	0.483	1.2	0.5	0.207	1.035	0.0137
RuPd	1.691	0.338	1.2	0.5	0.296	1.478	0.0196
Pd	1.734	0.347	1.2	0.5	0.270	1.441	0.0191
Pt	3.190	0.638	1.2	0.5	0.157	0.748	0.0104

calculation for the RuPd bimetallic catalyst as an example in supporting information, below Figure S2). Table 1 shows the summary of the calculations of STs for all monometallic and bimetallic catalysts with a constant metal to glycerol molar ratio of 1:200 for both reactor configurations. The catalytic activity of $RuPd/TiO_2$ catalyst was tested at a flow rate of 0.296 g glycerol h^{-1} with a ST of 1.7 $g_{catalyst}\,h\,g_{glycerol}{}^{-1}$ (Figure 6).

The activity of RuPd catalyst is slightly higher in the fixed bed reactor (30–35%) compared to the 6 h of reaction in a batch reactor (25–30%) under comparable reaction conditions (Figure 6). However, a 10% loss in CMB (G+L) was also observed in the continuous reactor (Figure S2). Similar to the batch reactor results, $RuPd/TiO_2$ catalyst is more stable compared to RuPt in the continuous reactor as well.

TGA analyses of the fresh and spent catalysts (after 1 and 16 h of reaction) showed that, even at high temperatures, the mass loss was almost insignificant, suggesting no poisoning or coke formation (see supporting information, Figure S3). Other reasons for the deactivation of supported metal catalysts could be (a) leaching of active metal component and/or (b) sintering of metal nanoparticles.[28] Understanding the mode of deactivation of these supported metal catalysts is crucial to design reactivation strategies. Hence, leaching studies were carried out by ICP analyses of the reaction mixture after hot filtration (supporting information Table S8). The results confirmed that significant leaching of metal components did not occur in these systems.

Fresh and spent Pd, RuPd and Ru catalysts were characterised by Scanning Transmission Electron Microscopy (STEM) (Figure 7) and the corresponding particle size distribution data are presented in the supporting information (Figure S4). The average particle size for the fresh monometallic Ru and the bimetallic RuPd catalysts were *ca.* 2.0 nm. The reason for the highest activity for both Ru and RuPd catalyst is the small metal particle size combined with excellent particle size distribution. We reported that the modified impregnation method gives very small Ru particles with excellent distribution.[13] The average particle size for the monometallic Pd catalyst was found to be 4.0 nm, which is much higher compared to the other catalysts. The particle size distribution data for the spent catalyst is very similar to that of the fresh catalysts (supporting information

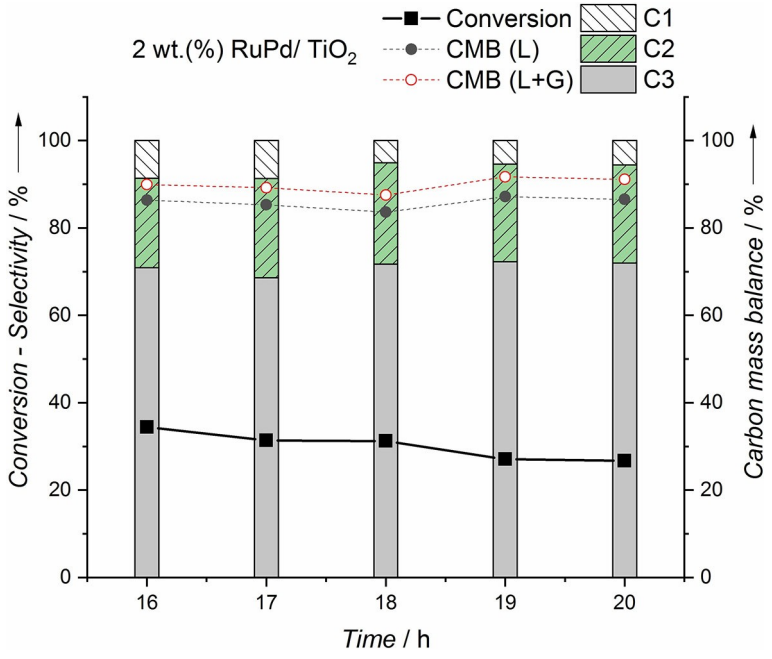

Figure 6. Stability studies for the $RuPd/TiO_2$ catalyst in the fixed-bed continuous flow reactor at 165 °C, 20 bar H_2, with a metal in catalyst to glycerol molar ratio of [1:200].

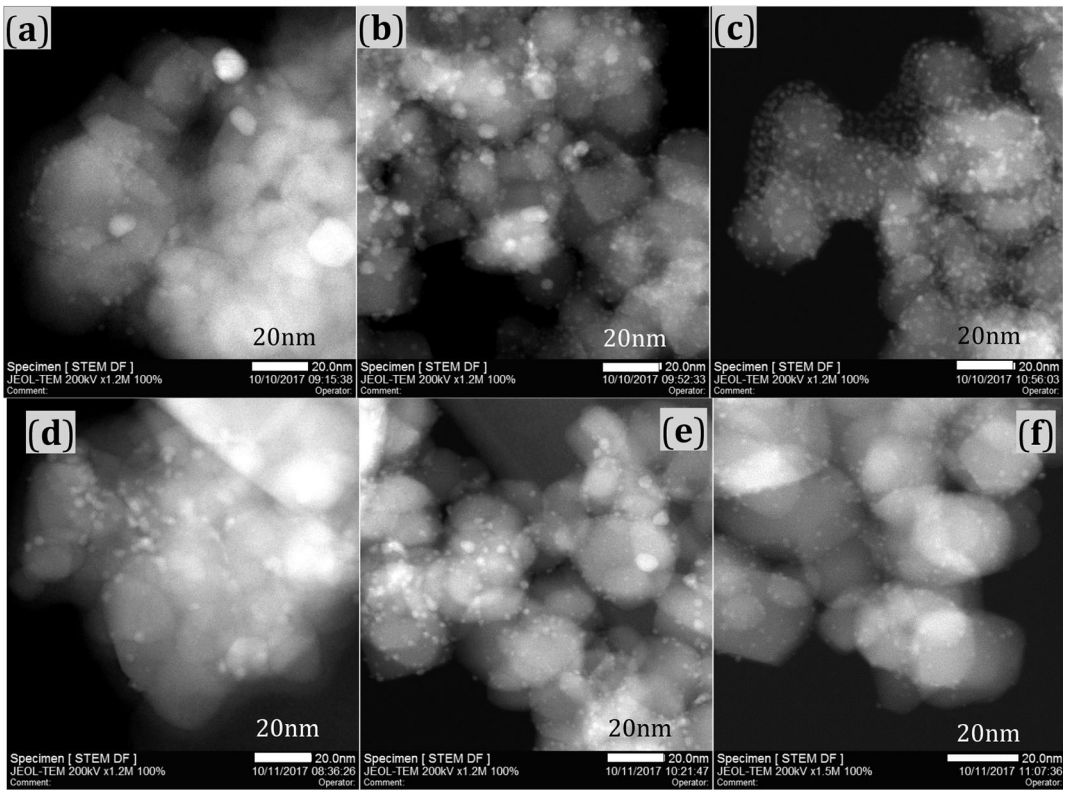

Figure 7. Top row: TEM bright field images of fresh (a) Pd/TiO_2, (b) $RuPd/ TiO_2$ and (c) Ru/ TiO_2 catalysts. Bottom row: TEM bright field images of the catalyst after 1st Reuse (d) Pd/TiO_2, (e) $RuPd/ TiO_2$ and (f) Ru/ TiO_2. The scale bars represent 20.0 nm.

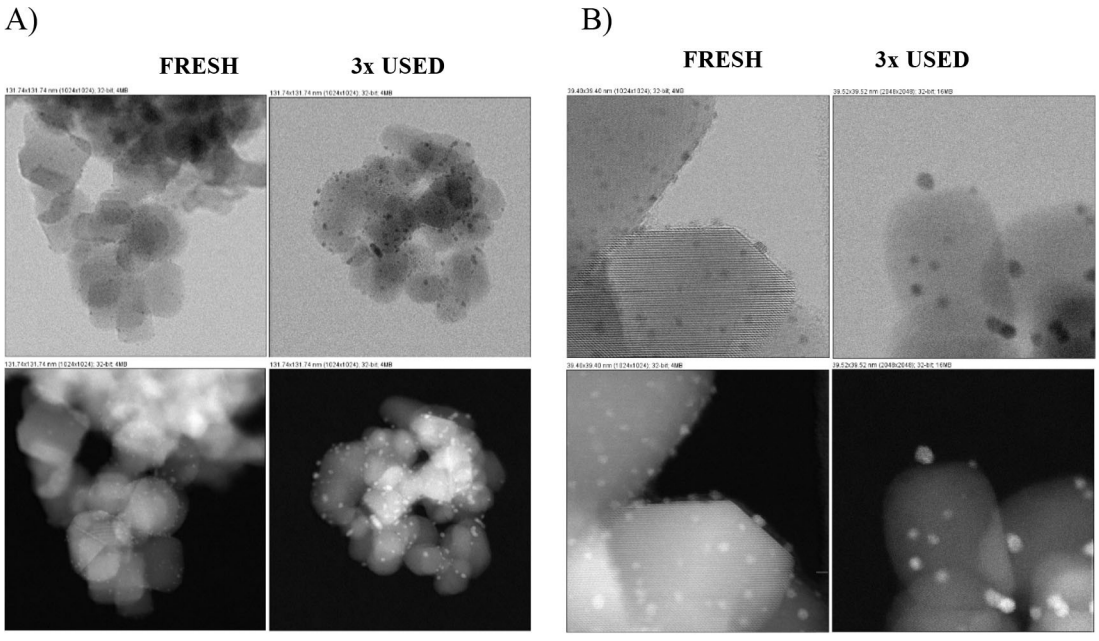

Figure 8. *STEM BF (top row) and HAADF (bottom row) micrographs of the 3 x times used RuPt on TiO_2 catalyst. Zoom boxes scaled A) 131.74x131.74 nm B) 39.52x39.52 nm.*

Figure S4). This correlates very well with the stability and reusability of all these catalysts.

In the case of $RuPt/TiO_2$ catalyst, the average particle size was found to be 1.5 nm (supporting information Figure S5), which is much smaller than the RuPd catalyst. Similarly,

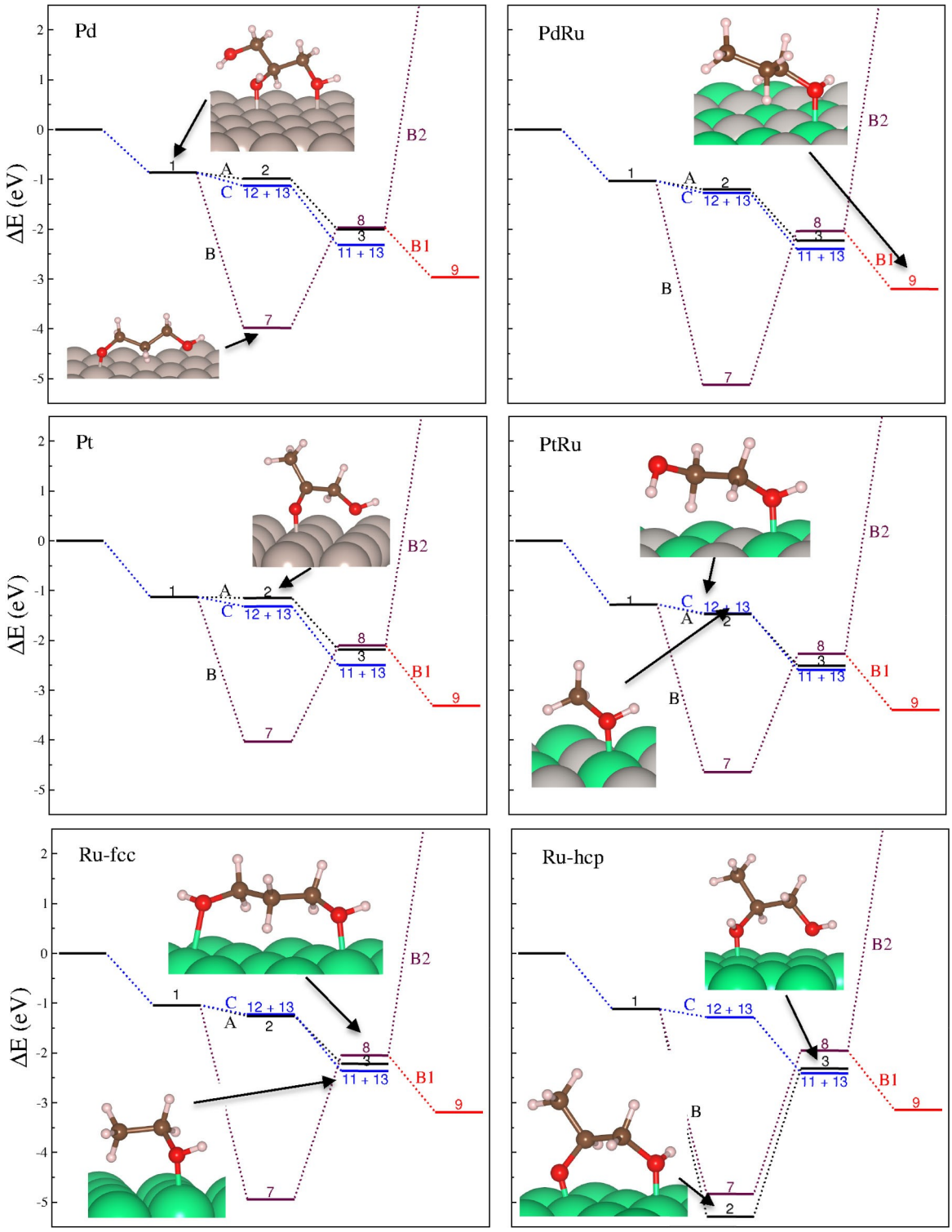

Figure 9. *Energy profiles for the dehydration (A and B) and C- C hydrogenolysis (C) mechanisms on Pd and RuPd (top), Pt and RuPt (centre) and Ru both fcc and hcp (down) according to Scheme 1. Representative structures of the different molecules on the most favourable adsorption site are given as inset. Note the characteristic bidentate character of acetol on Ru-hcp.*

monometallic Pt catalyst also showed a much smaller average particle size (1.8 nm). However, comparing the STEM data (HAADF and BF images in Figure 8 of the fresh and spent bimetallic RuPt catalyst (after 3 uses) we can see clear indication of sintering of bimetallic nanoparticles.

The average particle size of the spent catalyst increased by *ca.* 29% (from 1.6 nm to 2.25 nm). This explains the drop in the catalytic activity of $RuPt/TiO_2$ catalyst over reuse.

Fresh monometallic and bimetallic catalysts were characterised by XPS. The primary XPS regions of the elements employed are Pd 3d, Ru 3d and Pt 4f and the spectra are presented in supporting information (Figure S6). The Ru 3d signal suffers from overlap with the C 1s core-level (Spectra A in Figure S6), and chemical state information was extracted by means of fitting spectra taken from model compounds.[29] The use of such model compounds is important to avoid erroneous chemical state assignments since both metallic Ru and RuO_2 are conducting species and therefore exhibit an asymmetric peak shape. Spectra A exhibits both Ru^0 (280.2 eV) and Ru^{4+} (280.7 eV), with the remaining signal comprised of carbonaceous species.[29–30] Spectra B is characterised by the same Ru species as those in the Ru monometallic catalysts, but Pd is present in both metallic (335.2 eV) and oxide (336.7 eV) states,[30b,31] the metallic state is confirmed by the presence of satellites as reported in detail by Pillo *et al.*[31] The spectra in C again reveal both metallic and oxidic Ru species with binding energies identitical to, within the experimental condifence limits (±0.2 eV), whilst the Pt is present as Pt^0 (71.2 eV) and Pt^{2+} (72.3 eV). The observation of no significant shifts in binding energies suggests there is no discernable perturbation of the electronic states of the metals given the recorded values are akin to that of the pure compounds. However, the increased ruthenium oxide components for both RuPt and RuPd catalysts may be responsbile for the increased selectivity. Further studies are currently being done to prove this correlation. Table S9 shows the distribution of different species on the surface of the 3 fresh catalyst tested.

Finally, in order to rationalise the observed difference in catalytic behaviour between the monometallic and bimetallic catalysts and the mechanistic pathway favourable for each process, we have represented the relative energies along the early reactions mechanisms in Figure 9. Both, bimetallic (fcc) and monometallic Ru (hcp) behaves similarly. The surface intermediate favours the mechanism *via* dehydration **B**. Recently we reported that the surface acidity of $RuPd/TiO_2$ catalyst, through NH_3 and pyridine desorption studies, plays a key role during glycerol hydrogenolysis.[32] These acidic sites are responsible for this dehydration step. **B1** is not shown because it proceeds through an endothermic path compared to **B2**. Despite this, the hydrogenation of 3-hydroxypropanaldehyde is endothermic and hinders the pathway **B**. Thus, while pathway **B** is preferable in situations of energy conservation, pathways **A** and **C** are downhill in energy and therefore competing with **B**. Indeed, the surface intermediate 1,3-propanediol from pathway **B** has a higher relative energy than 1,2-propanediol and ethanol from pathways **A** and **C**, see Scheme 1. These arguments fit with the mechanistic profiles shown in Figure 9, where the intermediates are ethylene glycol and subsequent hydrogenation leads to an exothermic formation of CH_4. This dehydration followed by hydrogenation pathway has been widely reported for the hydrogenolysis of glycerol.[4a,33] We further studied the effect of the crystal structure and found that Ru-hcp largely stabilises acetol, following a pathway more favourable than **B**. Further detailed computational studies are necessary to compare different pathways.

Conclusions

Monometallic Ru/TiO_2 catalyst, prepared by modified impregnation, is extremely active for the liquid phase glycerol hydrogenolysis, however, producing mainly $<$C3 products because of effective C–C hydrogenolysis. Herein, we report that by adding a second metal such as Pd or Pt to Ru/TiO_2 catalyst, the selectivity for C3 products can be increased substantially. Bimetallic $RuPd/TiO_2$ and $RuPt/TiO_2$ suppress nearly 50% of the degradation products (C2 & C1) compared to the monometallic Ru/TiO_2 catalyst. Though both bimetallic catalysts have comparable catalytic properties such as activity and selectivity, $RuPd/TiO_2$ has a better stability. Spent $RuPt/TiO_2$ catalyst showed a substantial increase in the mean particle size indicating that the deactivation of this catalyst could be due to sintering of the bimetallic nanoparticles.

Acknowledgement

SGM, ASH and MS thank Cardiff University for the award of Global Challenges Research Funding and PhD studentship. MS, QH and AR thank Cardiff University for their University Research Fellowships. QH would also like to acknowledge the support by National Research Foundation (NRF) Singapore, under its NRF Fellowship (NRF-NRFF11-2019-0002). We also thank the EPSRC for the support through the EP/P005845/1 grant. We also acknowledge computing time on the facilities of Supercomputing Wales and the Advanced Research Computing @ Cardiff (ARCCA) at Cardiff University. All meta data generated during this research are openly available from the Cardiff University Research Portal at http://doi.org/10.17035/d.2021.0125886850

Conflict of Interest

The authors declare no conflict of interest.

Keywords: glycerol hydrogenolysis · bimetallic catalysts · C–C *vs* C–O cleavage · selectivity control

[1] a) N. Li, W. Wang, M. Zheng, T. Zhang, *Catalytic Hydrogenation for Biomass Valorization*, The Royal Society of Chemistry **2015**, pp. 22–51; b) A. Martin, U. Armbruster, I. Gandarias, P. L. Arias, *Eur. J. Lipid Sci. Technol.* **2013**, *115*, 9–27; c) D. Sun, Y. Yamada, S. Sato, W. Ueda, *Appl. Catal. B* **2016**, *193*, 75–92; d) Y. Wang, J. Zhou, X. Guo, *RSC Adv.* **2015**, *5*, 74611–74628; e) C.-H. Zhou, J. N. Beltramini, Y.-X. Fan, G. Q. Lu, *Chem. Soc. Rev.* **2008**, *37*, 527–549.
[2] a) A. Corma, S. Iborra, A. Velty, *Chem. Rev.* **2007**, *107*, 2411–2502; b) M. Besson, P. Gallezot, C. Pinel, *Chem. Rev.* **2014**, *114*, 1827–1870.
[3] C.-H. Zhou, X. Xia, C.-X. Lin, D.-S. Tong, J. Beltramini, *Chem. Soc. Rev.* **2011**, *40*, 5588–5617.

[4] a) Y. Nakagawa, K. Tomishige, *Catal. Sci. Technol.* **2011**, *1*, 179–190; b) M. J. Gilkey, B. Xu, *ACS Catal.* **2016**, *6*, 1420–1436.
[5] R. A. W. Johnstone, A. H. Wilby, I. D. Entwistle, *Chem. Rev.* **1985**, *85*, 129–170.
[6] S. Wang, K. Yin, Y. Zhang, H. Liu, *ACS Catal.* **2013**, *3*, 2112–2121.
[7] J. H. Sinfelt, *Acc. Chem. Res.* **1977**, *10*, 15–20.
[8] M. Sankar, N. Dimitratos, P. J. Miedziak, P. P. Wells, C. J. Kiely, G. J. Hutchings, *Chem. Soc. Rev.* **2012**, *41*, 8099–8139.
[9] F. Gao, D. W. Goodman, *Chem. Soc. Rev.* **2012**, *41*, 8009–8020.
[10] a) D. I. Enache, J. K. Edwards, P. Landon, B. Solsona-Espriu, A. F. Carley, A. A. Herzing, M. Watanabe, C. J. Kiely, D. W. Knight, G. J. Hutchings, *Science* **2006**, *311*, 362; b) R. J. Lewis, G. J. Hutchings, *ChemCatChem* **2019**, *11*, 298–308., c G. Dodekatos, L. Abis, S. J. Freakley, H. Tüysüz, G. J. Hutchings, *ChemCatChem* **2018**, *10*, 1351-1359
[11] D. D. Falcone, J. H. Hack, A. Y. Klyushin, A. Knop-Gericke, R. Schlögl, R. J. Davis, *ACS Catal.* **2015**, *5*, 5679–5695.
[12] W. Luo, M. Sankar, A. M. Beale, Q. He, C. J. Kiely, P. C. A. Bruijnincx, B. M. Weckhuysen, *Nat. Commun.* **2015**, *6*, 6540.
[13] J. B. Salazar, D. D. Falcone, H. N. Pham, A. K. Datye, F. B. Passos, R. J. Davis, *Appl. Catal. A* **2014**, *482*, 137–144.
[14] L. Ma, D. He, *Top. Catal.* **2009**, *52*, 834–844.
[15] E. P. Maris, W. C. Ketchie, M. Murayama, R. J. Davis, *J. Catal.* **2007**, *251*, 281–294.
[16] T. Miyazawa, Y. Kusunoki, K. Kunimori, K. Tomishige, *J. Catal.* **2006**, *240*, 213–221.
[17] M. Sankar, Q. He, M. Morad, J. Pritchard, S. J. Freakley, J. K. Edwards, S. H. Taylor, D. J. Morgan, A. F. Carley, D. W. Knight, C. J. Kiely, G. J. Hutchings, *ACS Nano* **2012**, *6*, 6600–6613.
[18] a) G. Kresse, J. Furthmüller, *Comput. Mater. Sci.* **1996**, *6*, 15–50; b) G. Kresse, J. Furthmüller, *Phys. Rev. B* **1996**, *54*, 11169–11186.
[19] J. P. Perdew, K. Burke, M. Ernzerhof, *Phys. Rev. Lett.* **1996**, *77*, 3865–3868.
[20] a) P. E. Blöchl, *Phys. Rev. B* **1994**, *50*, 17953–17979; b) G. Kresse, D. Joubert, *Phys. Rev. B* **1999**, *59*, 1758–1775.
[21] a) H. W. King, F. D. Manchester, *J. Phys. F* **1978**, *8*, 15–26; b) R. L. Clendenen, H. G. Drickamer, *J. Phys. Chem. Solids* **1964**, *25*, 865–868.
[22] H. J. Monkhorst, J. D. Pack, *Phys. Rev. B* **1976**, *13*, 5188–5192.
[23] G. Makov, M. C. Payne, *Phys. Rev. B* **1995**, *51*, 4014–4022.
[24] a) S. Grimme, *J. Comput. Chem.* **2006**, *27*, 1787–1799; b) S. Grimme, J. Antony, S. Ehrlich, H. Krieg, *J. Chem. Phys.* **2010**, *132*, 154104.
[25] a) E. S. Vasiliadou, A. A. Lemonidou, *Org. Process Res. Dev.* **2011**, *15*, 925–931; b) B. Li, J. Wang, Y. Yuan, H. Ariga, S. Takakusagi, K. Asakura, *ACS Catal.* **2011**, *1*, 1521–1528.
[26] P. Hirunsit, C. Luadthong, K. Faungnawakij, *RSC Adv.* **2015**, *5*, 11188–11197.
[27] E. Cao, M. Sankar, S. Firth, K. F. Lam, D. Bethell, D. K. Knight, G. J. Hutchings, P. F. McMillan, A. Gavriilidis, *Chem. Eng. J.* **2011**, *167*, 734–743.
[28] a) *Handbook of Heterogeneous Catalysis* **1997**, pp. 1263–1282; b) G. Boskovic, M. Baerns, *Basic Principles in Applied Catalysis* (Ed.: M. Baerns), Springer, Berlin, Heidelberg, **2004**, pp. 477–503.
[29] C. Elmasides, D. I. Kondarides, W. Grünert, X. E. Verykios, *J. Phys. Chem. B* **1999**, *103*, 5227–5239.
[30] a) D. J. Morgan, *Surf. Interface Anal.* **2015**, *47*, 1072–1079; b) E. A. Paoli, F. Masini, R. Frydendal, D. Deiana, C. Schlaup, M. Malizia, T. W. Hansen, S. Horch, I. E. L. Stephens, I. Chorkendorff, *Chem. Sci.* **2015**, *6*, 190–196.
[31] T. Pillo, R. Zimmermann, P. Steiner, S. Hüfner, *J. Phys. Condens. Matter* **1997**, *9*, 3987–3999.
[32] S. Guadix-Montero, A. Santos-Hernandez, A. Folli, M. Sankar, *Philos. Trans. R. Soc. A* **2020**, *378*, 20200055.
[33] a) Y. Amada, Y. Shinmi, S. Koso, T. Kubota, Y. Nakagawa, K. Tomishige, *Appl. Catal. B* **2011**, *105*, 117–127; b) Y. Kusunoki, T. Miyazawa, K. Kunimori, K. Tomishige, *Catal. Commun.* **2005**, *6*, 645–649.

Manuscript received: November 23, 2020
Revised manuscript received: December 20, 2020
Accepted manuscript online: December 22, 2020
Version of record online: February 2, 2021